Controllable X-Ray Pulse Trains from Enhanced Self-Amplified Spontaneous Emission

Joseph P. Duris,[1,*] James P. MacArthur,[1] James M. Glownia,[1] Siqi Li,[1] Sharon Vetter,[1] Alan Miahnahri,[1] Ryan Coffee,[1] Philippe Hering,[1] Alan Fry,[1] Marc E. Welch,[1] Alberto Lutman,[1] Franz-Josef Decker,[1] Dorian Bohler,[1] Jeremy A. Mock,[1] Chengcheng Xu,[1] Karl Gumerlock,[1] Justin E. May,[1] Antonio Cedillos,[1] Eugene Kraft,[1] Manuel A. Carrasco,[1] Brian E. Smith,[1] Logan R. Chieffo,[2] Joseph Z. Xu,[3] James P. Cryan,[1] Zhirong Huang,[1] Alexander Zholents,[3] and Agostino Marinelli[1,†]

[1]*SLAC National Accelerator Laboratory, Menlo Park, California 94025, USA*

[2]*Q-Peak, Inc., Bedford, Massachusetts 01730, USA*

[3]*Argonne National Laboratory, Lemont, Illinois 60439, USA*

(Received 18 September 2020; revised 1 December 2020; accepted 3 February 2021; published 12 March 2021)

We report the demonstration of optical compression of an electron beam and the production of controllable trains of femtosecond, soft x-ray pulses with the Linac Coherent Light Source (LCLS) free-electron laser (FEL). This is achieved by enhanced self-amplified spontaneous emission with a 2 μm laser and a dechirper device. Optical compression was achieved by modulating the energy of an electron beam with the laser and then compressing with a chicane, resulting in high current spikes on the beam which we observe to lase. A dechirper was then used to selectively control the lasing region of the electron beam. Field autocorrelation measurements indicate a train of pulses, and we find that the number of pulses within the train can be controlled (from 1 to 5 pulses) by varying the dechirper position and undulator taper. These results are a step toward attosecond spectroscopy with x-ray FELs as well as future FEL schemes relying on optical compression of an electron beam.

DOI: 10.1103/PhysRevLett.126.104802

X-ray free-electron lasers (XFEL) are the brightest sources of x-ray radiation [1] and have become indispensable tools for many scientific disciplines [2,3]. In an XFEL, the radiation is emitted by a high-brightness electron beam undergoing a collective instability which amplifies spontaneous radiation to a high-power saturation level. The FEL gain is strongly dependent on the properties of the electron beam, allowing the x-ray pulses to be shaped by manipulating the properties of the beam itself [4–14]. In particular, modulating with a wavelength comparable to the FEL coherence length enables temporal gating of the gain and thus provides control of the x-ray pulse envelope. Energy modulation introduced by laser-electron resonant interaction in a wiggler has been proposed as a temporal gating mechanism in schemes such as chirped-tapered free-electron lasers or enhanced self-amplified spontaneous emission (SASE) [15–18]. In these schemes the temporal profile of the x rays can be shortened to less than the standard cooperation length limit by accurately choosing the taper profile of the undulator to match the phase-space structure of the electron beam.

Bursts of radiation with durations of a few femtoseconds or shorter can create, control, and probe atomic-scale electron dynamics [19]. Dynamics can be probed via a pump-probe technique, where a pulse first prepares (or "pumps") a target system and a subsequent pulse probes the nonequilibrium state with a variable time delay. Soft x-ray pulses interact most strongly with core-level electrons, which are highly localized at the atomic centers in molecular systems, and therefore the binding energy and core-to-valence absorption spectrum of these tightly bound electrons provide a sensitive measure of localized electron density around various atoms in a molecule or molecular complex [20]. Moreover, nonlinear processes induced by short soft x-ray pulses produce localized electronic excitations [21–23]. Therefore, pairs of isolated attosecond soft x-ray pulses offer a route to preparing and probing electronic dynamics with atomic-site specificity.

Laser manipulation of electron beams offers a path for creating such pulses with soft x-ray FELs. Structures in the electron beam may emit coherent radiation in a wiggler magnet allowing the beam to self-modulate [24]. This has led to the generation of isolated subfemtosecond soft x-ray pulses [25,26], or even pairs of attosecond pulses [25,27]. The intensity of these pulses is 6 orders of magnitude higher than tabletop sources, making them capable of driving nonlinear x-ray matter interactions [28] and providing a new avenue for attosecond science.

Additionally, trains of phase-locked attosecond pulses can be used in an interferometric scheme to provide simultaneous time and energy resolution [29] and intense attosecond x-ray pulse trains can improve nonlinear, site-specific measurements. One way to produce pulse trains with greater fluxes is harmonic mixing with a seeded FEL,

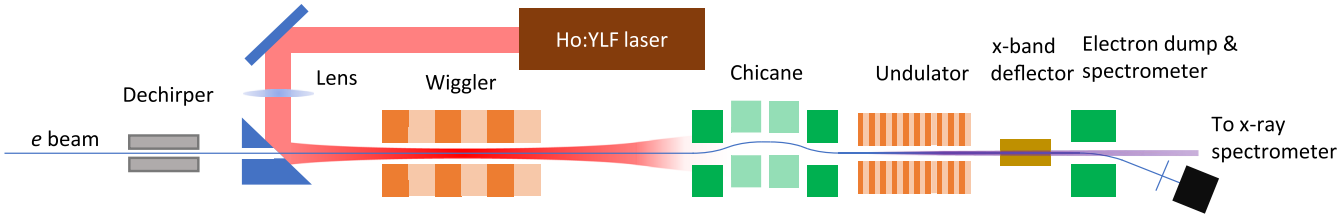

FIG. 1. Diagram of the experimental setup.

which has been shown to produce attosecond pulse trains with microjoule-level total pulse energies. However, this technique is currently limited to photon energies below 300 eV, preventing specific atomic-site excitations [30].

Another way to produce powerful, soft x-ray pulse trains is to apply a periodic modulation to the electron beam with a multicycle pulse from an external laser. When combined with the chirp-taper or enhanced self-amplified spontaneous emission (ESASE) schemes described above, this periodicity could enable production of trains of subfemtosecond soft x-ray pulses. This periodic modulation is also a prerequisite for mode-locked FEL schemes, whereby a series of chicane magnets between undulators delays the radiation by the periodicity of both the modulation and the FEL resonance. This results in a spectrum of equally spaced modes which are locked in phase and a train of pulses with durations shorter than the modulation periodicity [31–34] and even the possibility of few cycle, gigawatt, zeptosecond x-ray pulses [35] enabling the imaging and control of electron-nucleus interactions [36]. Periodic modulation also enables cascaded FEL amplification whereby an additional temporal gate, such as that employed by the fresh slice scheme [8], allows only one temporal mode to successively interact with each resonant part of the bunch. Such schemes promise terawatt x-ray pulses [37–41], necessary for atomic-scale single particle imaging [42].

In this Letter, we report an experimental demonstration of enhanced self-amplified spontaneous emission via optical compression of an electron beam with a 2 μm Ho:YLF laser at the Linac Coherent Light Source (LCLS). This compression generates a train of equally spaced, femtosecond x-ray pulses. We demonstrate that the number of pulses in the train can be controlled using a dechirper in combination with undulator taper. The results show a path toward controllable attosecond x-ray FEL pulse trains and is a step toward advanced FEL schemes relying on optical compression of an electron beam.

The experimental setup, depicted in Fig. 1, uses the LCLS electron beam, a Ho:YLF laser, a wiggler magnet, the soft x-ray self-seeding chicane [43], and the LCLS undulators to create the x-ray pulse train and then uses the dechirper to gate the pulse train. The LCLS linac was first tuned to produce 3.46 GeV electron beams with 150 pC of charge compressed to 2 kA. The longitudinal phase space of the electron beam, shown in Fig. 2(a), was resolved via temporal streaking with an x-band transverse deflecting cavity [44] and a dipole energy spectrometer.

A periodic energy modulation was imparted to the electron beam by copropagating it in the magnetic wiggler with a laser pulse with 5.5 mJ pulse energy and 3.3 ps FWHM pulse duration from the Ho:YLF laser [45,46]. The laser's pulse duration, measured with a single-shot autocorrelator, accommodates the electron beam's ~100 fs time of arrival jitter [59], and its 2053 nm wavelength yields current spikes with durations similar to the FEL coherence length. We estimate that the peak laser power delivered to the electron-laser-wiggler interaction region was 1–2 GW, and the intensity averaged over the length of the wiggler exceeded 0.4 GW/mm^2. This power is sufficient to impart an energy modulation comparable to the couple MeV slice energy spread of the LCLS electron beam [60]. The planar permanent magnet wiggler, designed and built by Argonne National Laboratory, consists of 6 periods, each 35 cm long, and a variable gap which we tuned to 16.8 mm (peak magnetic field of 1.03 T) for resonant interaction between the laser and electrons [46].

A periodic train of femtosecond duration, high current spikes was then created by delaying the beam by 800 fs

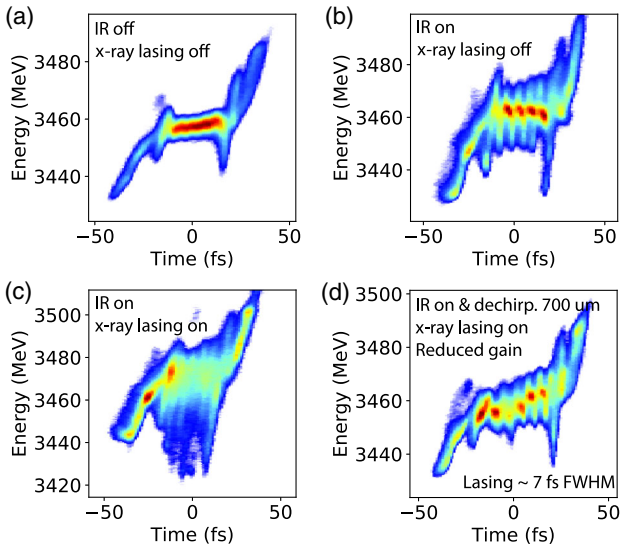

FIG. 2. Measured electron beam longitudinal phase space for (a) 2 μm laser off, (b) modulation with the 2 μm laser to produce high current spikes, (c) lasing on all spikes, and (d) single-spike lasing.

with a magnetic chicane, corresponding to an R_{56} of 480 μm, which converted the energy modulation into a density modulation. These spikes have peak currents exceeding the 2 kA input beam current and are as short as 1–2 fs, leading to a strong longitudinal space charge force which increases the energy spread of each spike as it propagates along the beam line [39]. Although the temporal resolution of the x-band transverse deflecting cavity is limited to ~2 fs, the large space charge induced energy spread of each spike shown in Fig. 2(b) is several times that of the laser modulation, indicating that the spikes are of order 1 fs based on a model of the space charge acting on the modulated beam.

We first verified that the laser modulation did not significantly affect the electron beam quality by investigating its affect on long-pulse lasing with a postsaturation undulator taper [46]. Figure 2(c) shows the measured longitudinal phase space of the modulated electron beam after lasing. Electrons decelerated while radiating appear as vertical bands of charge extending from the current spikes, indicating that electrons in the train of current spikes are the source of the radiation.

To study the regime of interest for this Letter, we then switched to short-pulse lasing by suppressing lasing for all but five undulators by kicking the beam off axis with steering magnets and then flattening the trajectory for the last five. We observed that the majority of the average x-ray pulse energy (67%) was produced in the fifth undulator, showing that the gain length was shorter than one undulator (< 3.3 m) and that this reduced undulator line was just long enough to allow the FEL power growth within each current spike to reach saturation. Postsaturation lasing can lengthen pulses as x rays slip past lasing current spikes in subsequent undulators so stopping the lasing just after saturation yields shorter pulses.

Additionally, we use the chirp-taper method [61,62] to maximize the FEL gain within the spikes. Between the chicane where the current spikes are formed and the last five undulators where the x-ray pulse train is created, 14 undulators delay the electrons with a FEL suppression beam trajectory, enhancing the current spikes' space charge energy chirps. We then selectively lase on each chirped current spike by linearly increasing the strength of each of the last five undulators [46] to maintain resonant interaction as generated radiation slips forward to more energetic electrons. This chirp-taper matching preferentially selects just the current spikes to lase as they are the only parts of the beam with the resonant energy chirp, and furthermore, the chirp increases the spectral bandwidth of the produced radiation, supporting shorter pulses [63].

Finally, we gate the pulse train with a time-correlated kick from a dechirper device to select a region of beam to lase containing a subset of the current spikes [8]. The dechirper is a corrugated metallic structure which induces strong transverse wakes when placed close to the electron beam, resulting in a time-dependent transverse kick [64,65]. The beam orbit may be controlled with corrector magnets and beam position monitors to keep one longitudinal point along the beam fixed on axis while the rest of the beam oscillates about the axis in a strong focusing lattice. The dechirper-induced time-dependent kick imparts a Gaussian shaped intensity envelope on the lasing and the width of this envelope may be controlled by varying the distance between the dechirper and electron beam [46]. Figure 2(d) shows an example of gating the ESASE spike lasing by the dechirper. A single band of electrons decelerated from a current spike near the center of the beam indicates that predominantly one current spike radiates. The measured shot-to-shot pulse energies observed in this case were 39 ± 21 μJ rms. The large relative fluctuations result from allowing only a few SASE temporal modes to grow.

We characterize the spectrum of the resulting FEL radiation using a soft x-ray spectrometer [66]. Figure 3 shows the measured spectral intensity $S(\omega)$ for various

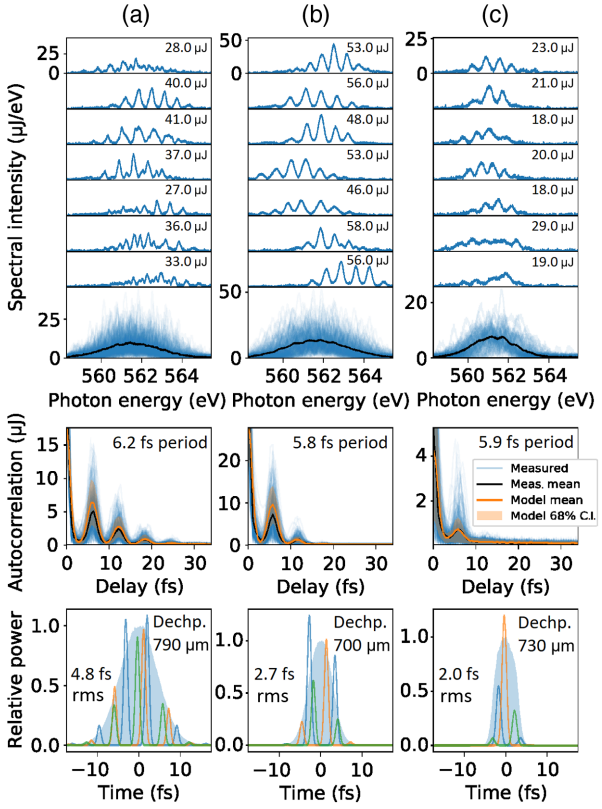

FIG. 3. X-ray FEL spectral diagnostics. Rows show (top) representative and average measured spectra, (middle) measured and modeled autocorrelation amplitudes, and (bottom) pulse profiles from three example shots (colored blue, orange, green) from the numerical model overlaid above the modeled intensity envelope (shaded) estimated from the 95th percentile of modeled powers. Columns (a) and (b) show two datasets where the dechirper kick is increased to reduce the pulse train length. Column (c) shows data for a case where the undulator taper was relaxed to reduce the FEL gain, allowing only one spike to lase.

dechirper and undulator configurations. The top row for each column shows several representative samples of the single-shot spectra above a panel showing superimposed and averaged spectra for that dataset. The periodic modulation of the spectrum results from interference between different pulses in the train. We controlled the pulse train gating via the dechirper and the FEL gain via the undulator taper to manipulate fringes in the online measured spectra.

In order to investigate the temporal structure of the radiation, we examine the autocorrelation of the electric field via the Fourier transform of the measured spectral intensity: $FT_\tau[S(\omega)] = \int_{-\infty}^{\infty} dt E(t)^* E(t-\tau) = A(\tau)$, where $E(t)$ is the electric field of the FEL radiation in the time domain. The electric field is composed of a series of short temporal pulses of energy U_j and duration σ_t, each spaced from the next by the modulation period τ_m: $E(t) = \sum_j^N \sqrt{U_j/\sqrt{2\pi}\sigma_t} e^{-(t-j\tau_m)^2/4\sigma_t^2 - i\omega_0(t-j\tau_m)+\phi_j}$. Here, ω_0 and ϕ_j are the central frequency and carrier envelope phase of each pulse. Note that each pulse's phase ϕ_j is random since each ESASE pulse within the train grew independently from shot noise. The dechirper modulates the pulse train with a Gaussian intensity envelope [46].

Although the phase of each pulse is random, the autocorrelation carries information about the pulse train envelope if its absolute value is averaged over many shots. To explain this point, consider a simplified case: the autocorrelation of a train of identical pulses with a Gaussian envelope and random phases. In this case the average autocorrelation amplitude is proportional to the product of the autocorrelations of a long train of identical pulses and the autocorrelation of the intensity envelope [46]:

$$A(\tau) \approx U_{\mathrm{net}} \sum_{s=-\infty}^{\infty} f_s e^{-s^2\tau_m^2/8\sigma_{\mathrm{env}}^2} e^{-(\tau-s\tau_m)^2/8\sigma_t^2}. \qquad (1)$$

Here, we have assumed that the pulse durations σ_t are short compared to the envelope width σ_{env}, and the energy of each pulse is given by $U_j = U_0 e^{-(j\tau_m - t_{\mathrm{env}})^2/2/\sigma_{\mathrm{env}}^2}$, where t_{env} is the peak of the dechirper envelope and $U_0 \approx U_{\mathrm{net}}\sqrt{2\pi}\sigma_{\mathrm{env}}/\tau_m$. Here, s iterates over peaks in the autocorrelation located at delay $\tau = s\tau_m$, the form factor $f_s = \delta_{s,0} + (1-\delta_{s,0})2^{-3/2}\pi^{1/4}\sqrt{\tau_m/\sigma_{\mathrm{env}}}$ weighs each peak, and $\delta_{j,k}$ is a Kronecker delta. The function $A(\tau)$ has a rms width proportional to the rms width of the pulse train envelope, and therefore can be used to recover the pulse train profile.

The same concept can be used to analyze our experimental data, although in this case one needs to account for additional effects such as the intensity fluctuation of individual pulses in the train and the temporal jitter of the laser modulation with respect to the e beam (resulting in a random phase of the pulse train with respect to the envelope).

In order to prepare a model to fit the observed data, we calculate the autocorrelations for a series of modeled shots, allowing the properties of each pulse to fluctuate. The average of 300 autocorrelation amplitudes are then fit to the mean of measured autocorrelation amplitudes for 300 shots via the method of least squares by varying the intensity envelope's Gaussian width σ_{env}, the pulse train periodicity τ_m, and the pulse duration σ_t. The method was verified with start-to-end simulations of a similar setup [46]. The resulting model envelope and a few example modeled shots are shown with different colors in the third row of Fig. 3.

From the data in Fig. 3, we measure the interpulse separation τ_m to vary between 5.9 and 6.2 fs for the different datasets. This periodicity differs significantly from the well-defined 6.8 fs period of the modulating laser as an energy chirp in the electron beam led to compression within the chicane. This offers a possibility to tune the periodicity of the pulse trains by controlling the rf chirp.

The fit pulse train envelope duration reduces from 4.8 fs rms to 2.7 fs as the dechirper to electron beam distance was decreased from 790 to 700 μm. The number of modeled pulses within each train is reduced as well, agreeing with the reduction in the number of peaks in the autocorrelation traces. To further cut the number of pulses in the train, we relaxed the taper [46] to reduce the FEL gain by deviating from the chirp-taper resonance. Figure 3(c) shows that this further diminished the number of peaks in the autocorrelation. The fit model yields a pulse train with an envelope duration of 2.0 fs rms and 6.0 fs FWHM. Since this envelope width is smaller than the periodicity of the train, most shots have a single dominant pulse with a small satellite pulse.

We estimate the energies of each pulse in this 1–2 pulse dataset by modeling each shot as the sum of two Gaussian pulses. The amplitude of the field autocorrelation of two Gaussian pulses has two peaks: one at zero delay and one at the pulse separation delay. The first peak's amplitude is the total pulse energy: $\tilde{A}(0) = U_+ + U_- = U_{\mathrm{net}}$, where U_+ is the dominant pulse's energy and $U_{\mathrm{sat}} = U_-$ is the satellite's energy. The amplitude of the second peak, located at the modulation period τ_{mod}, is the geometric mean of the two pulses' energies, $\tilde{A}(\tau_{\mathrm{mod}}) = \sqrt{U_+ U_-}$. For each shot in the dataset, we find the first side peak in the autocorrelation and estimate the pulse energies as $U_\pm = [\tilde{A}(0) \pm \sqrt{\tilde{A}(0)^2 - 4\tilde{A}(\tau_{\mathrm{mod}})^2}]/2$. The resulting total pulse energies and satellite energy ratios are shown scattered in Fig. 4(a). We observe that larger energy shots have smaller satellites, suggesting that we are operating the FEL near saturation and dominant pulses are those where the current spikes fall near the center of the dechirper-induced intensity envelope. Figure 4(b) shows that the majority (73%) of satellite pulses contain less than 10% of the pulse energy. Furthermore, 8% of all shots and 26% of shots with $U_{\mathrm{net}} > 10$ μJ have isolated pulses with negligible satellites ($< 1\%$ pulse energy).

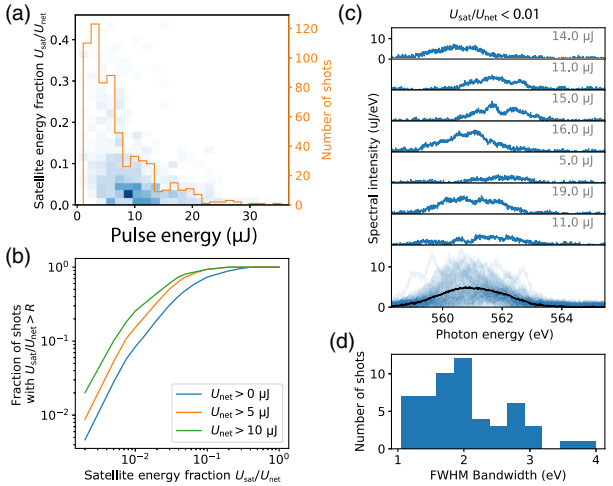

FIG. 4. Properties of the single pulse dataset. (a) A 2D histogram showing the density of shots (shading) versus total pulse energy and satellite pulse energy ratio. The orange 1D histogram shows number of shots versus total pulse energy (right-hand axis). (b) Cumulative distribution of shots versus satellite energy ratio for various pulse energies. (c) Spectra from 8% of shots with a dominant pulse containing $> 99\%$ of the pulse energy. (d) Histogram of spectral bandwidths for these isolated shots.

Measured spectra for the shots with an isolated pulse [Fig. 4(c)] exhibit negligible interference fringes in contrast with those in the full dataset [Fig. 3(c)]. These shots have FWHM bandwidths varying from 1.0 to 4.0 eV with an average of 2.0 eV [Fig. 4(d)]. We estimate the x-ray pulse energy chirp to be about 1.5 eV/fs from the energy chirp of the IR laser-induced current spikes on the electron beam. This suggests that most pulses have FWHM durations around 1 fs whereas some of the pulses with larger bandwidths may have subfemtosecond durations [46]. Increasing the amplitude of the electron beam energy modulation could increase the current and reduce the duration of the current spikes, driving stronger space charge induced chirps for greater bandwidths and attosecond pulse durations.

In conclusion, we demonstrated generation and control of soft x-ray pulse trains with a FEL via ESASE with an externally injected laser and a dechirper. By varying the dechirper and taper, we showed that the number of pulses in the train may be varied from 1 to 5 pulses. The periodicity of the pulses within the train may be controlled with rf chirp, and the frequency of the resulting radiation may be continuously tuned by varying the electron beam energy or undulator strength. Whereas the phase of each pulse in the train is random and independent in this experiment, self-seeding with monochromated SASE could establish a fixed phase relationship between each pulse in the train [33]. These results show a path toward future FEL setups relying on optical energy modulation.

The authors are grateful for the help of LCLS machine shop and laser technicians for helping to build the laser room and laser and to the engineers and technicians of ANL's magnetic device group for preparing the wiggler. The authors also greatly appreciate the LCLS operators' help in running the experiment and Zhaoheng Guo's help providing a start-to-end simulation of the LCLS beam with the dechirper. This work was supported by the Department of Energy, Office of Science under Contracts No. DE-AC02-76SF00515 and No. DE-AC02-06CH11357 as well as by the Department of Energy, Office of Basic Energy Science ADR Field Work Proposal No. 100317. J. P. C. was supported by the AMOS program in the Chemical Sciences, Geosciences, and Biosciences Division of Basic Energy Sciences at the Department of Energy. The development of the 2 μm laser source was supported by the Department of Energy's SBIR program under Contract No. DE-SC0007749.

*jduris@slac.stanford.edu
†marinelli@slac.stanford.edu

[1] P. Emma, R. Akre, J. Arthur, R. Bionta, C. Bostedt, J. Bozek, A. Brachmann, P. Bucksbaum, R. Coffee, F.-J. Decker *et al.*, First lasing and operation of an ångstrom-wavelength free-electron laser, Nat. Photonics **4**, 641 (2010).

[2] C. Bostedt, S. Boutet, D. M. Fritz, Z. Huang, H. J. Lee, H. T. Lemke, A. Robert, W. F. Schlotter, J. J. Turner, and G. J. Williams, Linac Coherent Light Source: The first five years, Rev. Mod. Phys. **88**, 015007 (2016).

[3] J. Rossbach, J. R. Schneider, and W. Wurth, 10 years of pioneering X-ray science at the Free-Electron Laser FLASH at DESY, Phys. Rep. **808**, 1 (2019).

[4] Y. Ding, C. Behrens, R. Coffee, F.-J. Decker, P. Emma, C. Field, W. Helml, Z. Huang, P. Krejcik, J. Krzywinski *et al.*, Generating femtosecond X-ray pulses using an emittance-spoiling foil in free-electron lasers, Appl. Phys. Lett. **107**, 191104 (2015).

[5] A. Marinelli, D. Ratner, A. Lutman, J. Turner, J. Welch, F.-J. Decker, H. Loos, C. Behrens, S. Gilevich, A. Miahnahri *et al.*, High-intensity double-pulse X-ray free-electron laser, Nat. Commun. **6**, 6369 (2015).

[6] A. Marinelli, R. Coffee, S. Vetter, P. Hering, G. N. West, S. Gilevich, A. A. Lutman, S. Li, T. Maxwell, J. Galayda, A. Fry, and Z. Huang, Optical Shaping of X-Ray Free-Electron Lasers, Phys. Rev. Lett. **116**, 254801 (2016).

[7] A. Marinelli, J. MacArthur, P. Emma, M. Guetg, C. Field, D. Kharakh, A. Lutman, Y. Ding, and Z. Huang, Experimental demonstration of a single-spike hard-X-ray free-electron laser starting from noise, Appl. Phys. Lett. **111**, 151101 (2017).

[8] A. A. Lutman, T. J. Maxwell, J. P. MacArthur, M. W. Guetg, N. Berrah, R. N. Coffee, Y. Ding, Z. Huang, A. Marinelli, S. Moeller *et al.*, Fresh-slice multicolour X-ray free-electron lasers, Nat. Photonics **10**, 745 (2016).

[9] S. Huang, Y. Ding, Y. Feng, E. Hemsing, Z. Huang, J. Krzywinski, A. A. Lutman, A. Marinelli, T. J. Maxwell, and

D. Zhu, Generating Single-Spike Hard X-Ray Pulses with Nonlinear Bunch Compression in Free-Electron Lasers, Phys. Rev. Lett. **119**, 154801 (2017).
[10] E. Hemsing, G. Stupakov, D. Xiang, and A. Zholents, Beam by design: Laser manipulation of electrons in modern accelerators, Rev. Mod. Phys. **86**, 897 (2014).
[11] G. Stupakov, Using the Beam-Echo Effect for Generation of Short-Wavelength Radiation, Phys. Rev. Lett. **102**, 074801 (2009).
[12] D. Xiang and G. Stupakov, Echo-enabled harmonic generation free electron laser, Phys. Rev. ST Accel. Beams **12**, 030702 (2009).
[13] D. Xiang and G. Stupakov, Enhanced tunable narrow-band THz emission from laser-modulated electron beams, Phys. Rev. ST Accel. Beams **12**, 080701 (2009).
[14] E. Hemsing, A. Knyazik, M. Dunning, D. Xiang, A. Marinelli, C. Hast, and J. B. Rosenzweig, Coherent optical vortices from relativistic electron beams, Nat. Phys. **9**, 549 (2013).
[15] E. L. Saldin, E. A. Schneidmiller, and M. V. Yurkov, Self-amplified spontaneous emission FEL with energy-chirped electron beam and its application for generation of attosecond x-ray pulses, Phys. Rev. ST Accel. Beams **9**, 050702 (2006).
[16] Z. Zhang, J. Duris, J. P. MacArthur, Z. Huang, and A. Marinelli, Double chirp-taper x-ray free-electron laser for attosecond pump-probe experiments, Phys. Rev. Accel. Beams **22**, 050701 (2019).
[17] J. Duris, Z. Zhang, J. MacArthur, Z. Huang, and A. Marinelli, Superradiant amplification in a chirped-tapered x-ray free-electron laser, Phys. Rev. Accel. Beams **23**, 020702 (2020).
[18] A. A. Zholents, Method of an enhanced self-amplified spontaneous emission for x-ray free electron lasers, Phys. Rev. ST Accel. Beams **8**, 040701 (2005).
[19] F. Krausz and M. Ivanov, Attosecond physics, Rev. Mod. Phys. **81**, 163 (2009).
[20] K. Siegbahn, Electron spectroscopy for atoms, molecules, and condensed matter, Rev. Mod. Phys. **54**, 709 (1982).
[21] S. Tanaka and S. Mukamel, Coherent X-Ray Raman Spectroscopy: A Nonlinear Local Probe for Electronic Excitations, Phys. Rev. Lett. **89**, 043001 (2002).
[22] S. Mukamel, D. Healion, Y. Zhang, and J. D. Biggs, Multidimensional Attosecond Resonant X-Ray Spectroscopy of Molecules: Lessons from the Optical Regime, Annu. Rev. Phys. Chem. **64**, 101 (2013).
[23] J. D. Biggs, Y. Zhang, D. Healion, and S. Mukamel, Two-dimensional stimulated resonance Raman spectroscopy of molecules with broadband x-ray pulses, J. Chem. Phys. **136**, 174117 (2012).
[24] J. P. MacArthur, J. Duris, Z. Zhang, A. Lutman, A. Zholents, X. Xu, Z. Huang, and A. Marinelli, Phase-Stable Self-Modulation of an Electron Beam in a Magnetic Wiggler, Phys. Rev. Lett. **123**, 214801 (2019).
[25] J. Duris, S. Li, T. Driver, E. G. Champenois, J. P. MacArthur, A. A. Lutman, Z. Zhang, P. Rosenberger, J. W. Aldrich, R. Coffee *et al.*, Tunable isolated attosecond X-ray pulses with gigawatt peak power from a free-electron laser, Nat. Photonics **14**, 30 (2020).
[26] Z. Zhang, J. Duris, J. P. MacArthur, A. Zholents, Z. Huang, and A. Marinelli, Experimental demonstration of enhanced self-amplified spontaneous emission by photocathode temporal shaping and self-compression in a magnetic wiggler, New J. Phys. **22**, 083030 (2020).
[27] Z. Zhang, J. Duris, J. P. MacArthur, Z. Huang, and A. Marinelli, Double chirp-taper x-ray free-electron laser for attosecond pump-probe experiments, Phys. Rev. Accel. Beams **22**, 050701 (2019).
[28] J. T. O'Neal *et al.*, Electronic Population Transfer via Impulsive Stimulated X-Ray Raman Scattering with Attosecond Soft-X-Ray Pulses, Phys. Rev. Lett. **125**, 073203 (2020).
[29] J. Mauritsson, P. Johnsson, E. Mansten, M. Swoboda, T. Ruchon, A. L'Huillier, and K. J. Schafer, Coherent Electron Scattering Captured by an Attosecond Quantum Stroboscope, Phys. Rev. Lett. **100**, 073003 (2008).
[30] P. K. Maroju, C. Grazioli, M. Di Fraia, M. Moioli, D. Ertel, H. Ahmadi, O. Plekan, P. Finetti, E. Allaria, L. Giannessi *et al.*, Attosecond pulse shaping using a seeded free-electron laser, Nature (London) **578**, 386 (2020).
[31] N. R. Thompson and B. W. J. McNeil, Mode Locking in a Free-Electron Laser Amplifier, Phys. Rev. Lett. **100**, 203901 (2008).
[32] E. Kur, D. J. Dunning, B. W. J. McNeil, J. Wurtele, and A. A. Zholents, A wide bandwidth free-electron laser with mode locking using current modulation, New J. Phys. **13**, 063012 (2011).
[33] D. Xiang, Y. Ding, T. Raubenheimer, and J. Wu, Mode-locked multichromatic x rays in a seeded free-electron laser for single-shot x-ray spectroscopy, Phys. Rev. ST Accel. Beams **15**, 050707 (2012).
[34] C. Feng, J. Chen, and Z. Zhao, Generating stable attosecond x-ray pulse trains with a mode-locked seeded free-electron laser, Phys. Rev. ST Accel. Beams **15**, 080703 (2012).
[35] D. J. Dunning, B. W. J. McNeil, and N. R. Thompson, Few-Cycle Pulse Generation in an X-Ray Free-Electron Laser, Phys. Rev. Lett. **110**, 104801 (2013).
[36] S. Kishimoto, Y. Yoda, M. Seto, Y. Kobayashi, S. Kitao, R. Haruki, T. Kawauchi, K. Fukutani, and T. Okano, Observation of Nuclear Excitation by Electron Transition in ^{197}Au with Synchrotron X Rays and an Avalanche Photodiode, Phys. Rev. Lett. **85**, 1831 (2000).
[37] T. Tanaka, Proposal for a Pulse-Compression Scheme in X-Ray Free-Electron Lasers to Generate a Multiterawatt, Attosecond X-Ray Pulse, Phys. Rev. Lett. **110**, 084801 (2013).
[38] T. Tanaka, Y. W. Parc, Y. Kida, R. Kinjo, C. H. Shim, I. S. Ko, B. Kim, D. E. Kim, and E. Prat, Using irregularly spaced current peaks to generate an isolated attosecond X-ray pulse in free-electron lasers, J. Synchrotron Radiat. **23**, 1273 (2016).
[39] S. Huang, Y. Ding, Z. Huang, and G. Marcus, Generation of subterawatt-attosecond pulses in a soft x-ray free-electron laser, Phys. Rev. Accel. Beams **19**, 080702 (2016).
[40] Z. Wang, C. Feng, and Z. Zhao, Generating isolated terawatt-attosecond x-ray pulses via a chirped-laser-enhanced high-gain free-electron laser, Phys. Rev. Accel. Beams **20**, 040701 (2017).

[41] S. Kumar, A. S. Landsman, and D. E. Kim, Terawatt-isolated attosecond x-ray pulse using a tapered x-ray free electron laser, Appl. Sci. **7**, 614 (2017).
[42] A. Aquila *et al.*, The linac coherent light source single particle imaging road map, Struct. Dyn. **2**, 041701 (2015).
[43] D. Ratner *et al.*, Experimental Demonstration of a Soft X-Ray Self-Seeded Free-Electron Laser, Phys. Rev. Lett. **114**, 054801 (2015).
[44] C. Behrens, F.-J. Decker, Y. Ding, V. Dolgashev, J. Frisch, Z. Huang, P. Krejcik, H. Loos, A. Lutman, T. Maxwell *et al.*, Few-femtosecond time-resolved measurements of X-ray free-electron lasers, Nat. Commun. **5**, 3762 (2014).
[45] A. Dergachev, High-energy, kHz-rate, picosecond, 2-μm laser pump source for mid-IR nonlinear optical devices, in *Solid State Lasers XXII: Technology and Devices*, Vol. 8599, edited by W. A. Clarkson and R. Shori (International Society for Optics and Photonics, San Francisco, 2013), pp. 46–59, http://dx.doi.org/10.1117/12.2001386.
[46] See Supplemental Material at http://link.aps.org/supplemental/10.1103/PhysRevLett.126.104802 for more experimental details, which includes Refs. [47–58].
[47] K. Murari, H. Cankaya, P. Li, A. Ruehl, I. Hartl, and F. X. Kärtner, 1.2 mJ, 1 kHz, ps-pulses at 2.05 μm from a Ho:fibre / Ho:YLF laser, in *Proceedings of the 2014 Europhoton Conference* (OSA, Neuchatel, 2014), http://dx.doi.org/10.13140/RG.2.1.3867.9923.
[48] M. Hemmer, D. Sánchez, M. Jelínek, V. Smirnov, H. Jelinkova, V. Kubeček, and J. Biegert, 2-μm wavelength, high-energy Ho:YLF chirped-pulse amplifier for mid-infrared OPCPA, Opt. Lett. **40**, 451 (2015).
[49] U. Elu, T. Steinle, D. Sánchez, L. Maidment, K. Zawilski, P. Schunemann, U. Zeitner, C. Simon-Boisson, and J. Biegert, Table-top high-energy 7 μm OPCPA and 260 mJ Ho:YLF pump laser, Opt. Lett. **44**, 3194 (2019).
[50] O. E. Martinez, J. P. Gordon, and R. L. Fork, Negative group-velocity dispersion using refraction, J. Opt. Soc. Am. A **1**, 1003 (1984).
[51] E. Treacy, Optical pulse compression with diffraction gratings, IEEE J. Quantum Electron. **5**, 454 (1969).
[52] J. P. MacArthur, Electron beam manipulations at the angstrom level and attosecond timescale for x-ray FELS, Ph.D. thesis, Stanford University, Stanford, CA, 2020, https://search.proquest.com/openview/49febbf06ec4f67a86fa9b01b5cdb804/1?pq-origsite=gscholar&cbl=18750&diss=y.
[53] A. Zholents and K. Holldack, Energy modulation of the electrons by the laser field in the wiggler magnet: Analysis and experiment, in *Proceedings of the 28th International Free Electron Laser Conference (FEL '06), Berlin* (The BESSY FEL Conference Team, Berlin, 2006), http://accelconf.web.cern.ch/f06/PAPERS/THPPH059.PDF.
[54] P. Baxevanis, Z. Huang, and G. Stupakov, Effect of an angular trajectory kick in a high-gain free-electron laser, Phys. Rev. Accel. Beams **20**, 040703 (2017).
[55] T. Tanaka, H. Kitamura, and T. Shintake, Consideration on the BPM alignment tolerance in X-ray FELs, Nucl. Instrum. Methods Phys. Res., Sect. A **528**, 172 (2004).
[56] Y. Wang and M. Borland, Pelegant: A parallel accelerator simulation code for electron generation and tracking, in *AIP Conference Proceedings*, Vol. 877 (American Institute of Physics, New York, 2006), pp. 241–247, https://doi.org/10.1063/1.2409141.
[57] S. Reiche, GENESIS 1.3: a fully 3D time-dependent FEL simulation code, Nucl. Instrum. Methods Phys. Res., Sect. A **429**, 243 (1999).
[58] C. Pellegrini, A. Marinelli, and S. Reiche, The physics of x-ray free-electron lasers, Rev. Mod. Phys. **88**, 015006 (2016).
[59] J. M. Glownia, J. Cryan, J. Andreasson, A. Belkacem, N. Berrah, C. Blaga, C. Bostedt, J. Bozek, L. DiMauro, L. Fang *et al.*, Time-resolved pump-probe experiments at the LCLS, Opt. Express **18**, 17620 (2010).
[60] D. Ratner, C. Behrens, Y. Ding, Z. Huang, A. Marinelli, T. Maxwell, and F. Zhou, Time-resolved imaging of the microbunching instability and energy spread at the Linac Coherent Light Source, Phys. Rev. ST Accel. Beams **18**, 030704 (2015).
[61] E. L. Saldin, E. A. Schneidmiller, and M. V. Yurkov, Self-amplified spontaneous emission FEL with energy-chirped electron beam and its application for generation of attosecond x-ray pulses, Phys. Rev. ST Accel. Beams **9**, 050702 (2006).
[62] L. Giannessi *et al.*, Self-Amplified Spontaneous Emission Free-Electron Laser with an Energy-Chirped Electron Beam and Undulator Tapering, Phys. Rev. Lett. **106**, 144801 (2011).
[63] P. Baxevanis, J. Duris, Z. Huang, and A. Marinelli, Time-domain analysis of attosecond pulse generation in an x-ray free-electron laser, Phys. Rev. Accel. Beams **21**, 110702 (2018).
[64] Z. Zhang, K. Bane, Y. Ding, Z. Huang, R. Iverson, T. Maxwell, G. Stupakov, and L. Wang, Electron beam energy chirp control with a rectangular corrugated structure at the Linac Coherent Light Source, Phys. Rev. ST Accel. Beams **18**, 010702 (2015).
[65] J. Zemella, K. Bane, A. Fisher, M. Guetg, Z. Huang, R. Iverson, P. Krejcik, A. Lutman, T. Maxwell, A. Novokhatski, G. Stupakov, Z. Zhang, M. Harrison, and M. Ruelas, Measurements of wake-induced electron beam deflection in a dechirper at the Linac Coherent Light Source, Phys. Rev. Accel. Beams **20**, 104403 (2017).
[66] P. Heimann *et al.*, Linac Coherent Light Source soft x-ray materials science instrument optical design and monochromator commissioning, Rev. Sci. Instrum. **82**, 093104 (2011).